

# CIRCULAR-ORBIT MAINTENANCE STRATEGIES FOR PRIMITIVE BODY ORBITERS

Mark S. Wallace and Stephen Broschart\*

For missions to smaller primitive bodies, solar radiation pressure (SRP) is a significant perturbation to Keplerian dynamics. For most orbits, SRP drives large oscillations in orbit eccentricity, which leads to large perturbations from the irregular gravity field at periapsis. Ultimately, chaotic motion results that often escapes or impacts that body. This paper presents an orbit maintenance strategy to keep the orbit eccentricity small, thus avoiding the destabilizing secondary interaction with the gravity field. An estimate of the frequency and magnitude of the required maneuvers as a function of the orbit and body parameters is derived from the analytic perturbation equations.

## INTRODUCTION

For missions to smaller primitive bodies, solar radiation pressure (SRP) is a significant perturbation to Keplerian dynamics. For most orbits, SRP drives large oscillations in orbit eccentricity, which leads to large perturbations from the irregular gravity field at periapsis. Ultimately, chaotic motion results that often escapes or impacts that body. This paper presents a pair of similar orbit maintenance strategies to keep the orbit eccentricity small, thus avoiding the destabilizing secondary interaction with the gravity field. An estimate of the frequency and magnitude of the required maneuvers as a function of the orbit and body parameters is derived from the analytic perturbation equations. Numerical results of the application of control laws designed to fix maneuver targets or maneuver schedules derived from the analytic equations applied to full-ephemeris simulations are also shown.

## DYNAMICS OF NEAR-CIRCULAR ORBITS

The mean effect of a simple, anti-sun SRP model on a set of orbital elements has been described using the following equations:<sup>1</sup>

$$\dot{\lambda} = -\frac{C_g e}{\sqrt{1-e^2}} \sin \omega \sin \lambda - \dot{N} \quad (1)$$

$$\frac{d}{dt} i = -\frac{C_g e}{\sqrt{1-e^2}} \cos \omega \sin i \sin \lambda \quad (2)$$

$$\dot{e} = -C_g \sqrt{1-e^2} (\sin \omega \cos \lambda + \cos \omega \cos i \sin \lambda) \quad (3)$$

---

\* Mission Design Engineers, Mission Design & Navigation Section, Jet Propulsion Laboratory, California Institute of Technology, 4800 Oak Grove Dr. Pasadena, CA 91109, M/S 301-121

$$\dot{\omega} = -\frac{C_g \sqrt{1-e^2}}{e} (\cos \omega \cos \lambda - \sin \omega \cos i \sin \lambda) - (\dot{\lambda} + \dot{N}) \cos i \quad (4)$$

$$\dot{a} = 0 \quad (5)$$

$$C_g = \frac{3G_1}{2BR^2} \sqrt{\frac{a}{\mu}} \quad (6)$$

Where:

- $e$  Eccentricity
- $a$  Semi-major axis
- $i$  Inclination
- $\omega$  Argument of periapsis
- $\lambda$  Node of the orbit relative to the sun line
- $\dot{N}$  Instantaneous orbital rate of the central body (asteroid, comet) about the sun
- $G_1$  The solar constant  $\approx 10^{17}$  Newton
- $B$  The effective spacecraft mass/area ratio
- $R$  The central body (asteroid, comet) distance from the sun
- $\mu$  The gravitational parameter of the central body (asteroid, comet)
- $C_g$  The solar-pressure / gravity ratio parameter.
- $\dot{x}$  or  $\frac{d}{dt}x$  The time rate of change of the parameter  $x$

For orbits with sufficiently small eccentricities, equation 1 approaches the orbital rate of the asteroid (or comet) about the sun and equation 2 becomes small relative to the remaining terms. Equation 2 becomes even smaller (since  $e$  is non-zero, but small compared to  $\sqrt{1-e^2}$ ) if the inclination is near polar. While a polar orbit assumption is not strictly necessary for the derivation, it does make for a cleaner solution. Making the small-eccentricity assumption, then, equations 1, 2, and 4 simplify:

$$\frac{d}{dt}i \approx 0 \quad (11)$$

$$\dot{\lambda} \approx -\dot{N} \quad (12)$$

$$\dot{\omega} = -\frac{C_g \sqrt{1-e^2}}{e} (\cos \omega \cos \lambda - \sin \omega \cos i \sin \lambda). \quad (13)$$

This implies that, so long as the eccentricity remains small, the orbit plane is essentially inertial and that shape and orientation of the orbit within the plane are oscillating under the influence of solar radiation pressure.

The presence of the eccentricity in the denominator of equation 13 presents a problem for near-circular orbits that can be eliminated by recasting the eccentricity and argument of periapsis in terms of the components of the eccentricity vector:  $e_x$  and  $e_y$ . By doing so,

$$e_x = e \cos \omega \quad (14)$$

$$e_y = e \sin \omega, \quad (15)$$

the time rates of change become:

$$\dot{e}_x = \dot{e} \cos \omega - e \dot{\omega} \sin \omega \quad (16)$$

$$\dot{e}_y = \dot{e} \sin \omega + e \dot{\omega} \cos \omega. \quad (17)$$

By substituting equations 3 and 13 into equations 16 and 17, it becomes possible to eliminate the magnitude of the eccentricity from the denominator of equation 13, and a pair of useful equations emerges:

$$\dot{e}_x = -C_g \sqrt{1 - e^2} \cos i \sin \lambda \quad (18)$$

$$\dot{e}_y = -C_g \sqrt{1 - e^2} \cos \lambda. \quad (19)$$

For an exactly polar orbit, these two equations simplify greatly:

$$\dot{e}_x = 0 \quad (20)$$

$$\dot{e}_y = -C_g \sqrt{1 - e^2} \cos \lambda \quad (21)$$

These, then, imply, that the eccentricity vector runs exactly “up” or “down” in a polar plot of eccentricity and argument of periapsis (“ $e$ - $\omega$  space”), depending on the sign of the cosine of the hour-angle of the orbit plane. Further, this motion will reverse itself as the generally inertial orbit plane goes through an edge-on orientation relative to the sun and the sign of the cosine flips. However, this reversal occurs on a time scale comparable to the orbit period of the asteroid or comet about the sun. Even a non-polar orbit will see a similar very-long-period. The more polar it is, the smaller the component of that motion in the horizontal direction. Recall that for this formulation, the coordinate frame used is a sun-asteroid synodic (or sun-relative) frame, and the inclination is measured relative to the orbit plane of the asteroid or comet about the sun and not necessarily the equator of the body. As such, it is much more likely that the orbit evolution would be better described by equations 18 and 19 than 20 and 21.

The time constant of the oscillation, as mentioned earlier, is equal to the orbit period of the asteroid or comet about the sun. The magnitude is a function of  $C_g$  and thus the specific body, the orbit being studied, and the assumed spacecraft. If we consider the case of a spacecraft in orbit about Tempel 1 ( $\mu = 4479 \text{ m}^3/\text{sec}^2$ ) and making reasonable assumptions about the spacecraft mass/area ratio ( $B = 32 \text{ kg/m}^2$ ) and the semi-major axis of the orbit ( $a = 24 \text{ km}$ ), the parameter  $C_g$  has a large enough value ( $3 \times 10^{-8} \text{ Hz}$ ) even at 4 AU to increase the eccentricity of an initially circular orbit to 0.018 in a week, thus lowering periapsis by 0.44 km in a worst-case hour-angle ( $\lambda = 0^\circ$ , corresponding to an edge-on orientation). At Tempel 1’s perihelion distance of 1.5 AU, the eccentricity change increases by an order of magnitude. Thus regular maintenance would be required to maintain the nearly circular orbit.

If we assume that the orbit maintenance frequency is much larger than the rate of change of the orbital hour angle ( $\lambda$ ) and the SRP/Gravity parameter ( $C_g$ ), such that they can be considered constant, and further assume that eccentricity is small such that  $\sqrt{1 - e^2} \approx 1$ , then equations 18 and 19 reduce to simple constant rates:

$$\dot{e}_x = -C_g \cos i \sin \lambda \quad (22)$$

$$\dot{e}_y = -C_g \cos \lambda \quad (23)$$

The implication of this much-simplified model is that the eccentricity and argument of periapsis will evolve in the same relative way, given the same initial inclination, hour angle, and solar distance, regardless of their initial values, provided the time scale is short enough and the orbit remains sufficiently circular.

Given the fundamental assumptions that the orbit eccentricity is small, the main result of the derivation above is that the orbit plane is essentially fixed inertially and that the solar radiation pressure force causes the orbit shape and orientation within the plane, but not its size, to vary linearly at a constant rate. This rate, captured in equations 22 and 23, is a function of the orbit size ( $a$ ), inclination ( $i$ ), and hour angle ( $\lambda$ ) as well as the ratio of solar radiation pressure to central body gravity ( $C_g$ ).

## COMPARISON OF THE MODEL TO INTEGRATED TRAJECTORIES

For this, and all other numerical tests, an example system about Tempel 1 was developed, consistent with our best understanding of its ephemeris<sup>2</sup> and shape.<sup>3</sup> The shape model was transformed<sup>4</sup> into a degree-and-order 12 spherical harmonic gravity field using a constant density of 0.6 g/cc. The osculating initial states, relative to the Tempel 1 pole and in the sun-line frame used to derive Equations 1-6, are detailed in Table 1. Left to evolve on its own, this initial state is driven close enough to a lobe in the Tempel 1 gravity field that it is ejected from orbit.

**Table 1: Initial State Used for All Numerical Tests**

| Parameter             | Value (Pole)   | Value (Sun-Line) | Unit |
|-----------------------|----------------|------------------|------|
| Initial Epoch         | 24 August 2020 |                  | TDB  |
| Semi-Major Axis       | 22.5           | 22.5             | km   |
| Eccentricity          | 0.02           | 0.02             |      |
| Inclination           | 75.0           | 67.2             | deg  |
| Argument of Periapsis | 255.0          | 264.0            | deg  |

The first check to perform is to determine if Equations 1-6 do a “good enough” job describing the evolution of the orbit from Table 1. The easiest way to do that is to propagate the orbit and inspect the evolution of the elements. Figure 1 shows the results of a 10-day propagation. As can be seen there, the semi-major axis is essentially constant, though with a large multi-frequency oscillation. The ascending node, which is a component of the hour angle,  $\lambda$ , shows the expected nearly-linear behavior. The inclination is also showing a secular variation during these 10 days. However, the 0.01 deg/day inclination rate is several orders of magnitude slower than the 20 deg/day apsidal rate. That is consistent with the claim that the inclination rate approaches zero as the eccentricity does. Based on this, the dynamics of Tempel 1 are apparently sufficiently described by the base equations used in the derivation of the controller.

But, before we can address the issue of whether or not Equations 22-23 describe the evolution of the eccentricity and argument of periapsis, we must first determine the nature of the SRP-Gravity parameter,  $C_g$ . The spacecraft *effective* mass/area ratio,  $B$ , is not simply the mass of the spacecraft divided by its cross-sectional area normal to the sun-line. It must take into account diffuse and specular reflection. Given a system to perform the full-dynamical propagation, the easiest way to calculate  $C_g$  is using Equation 24:

$$C_g(t) = \frac{3F_s}{2m} \sqrt{\frac{a}{\mu}} \quad (24)$$

where  $F_s$  is the magnitude of the solar pressure force parallel to the sun-line,  $m$  is the mass of the spacecraft, and the other symbols are as previously defined. It should be noted that in this formulation,  $C_g$  is transformed to a time-varying value. The distance to the sun isn't a constant, the cross-sectional area of the spacecraft isn't necessarily constant, and the osculating semi-major axis varies. Ideally, the combined value is nearly constant.

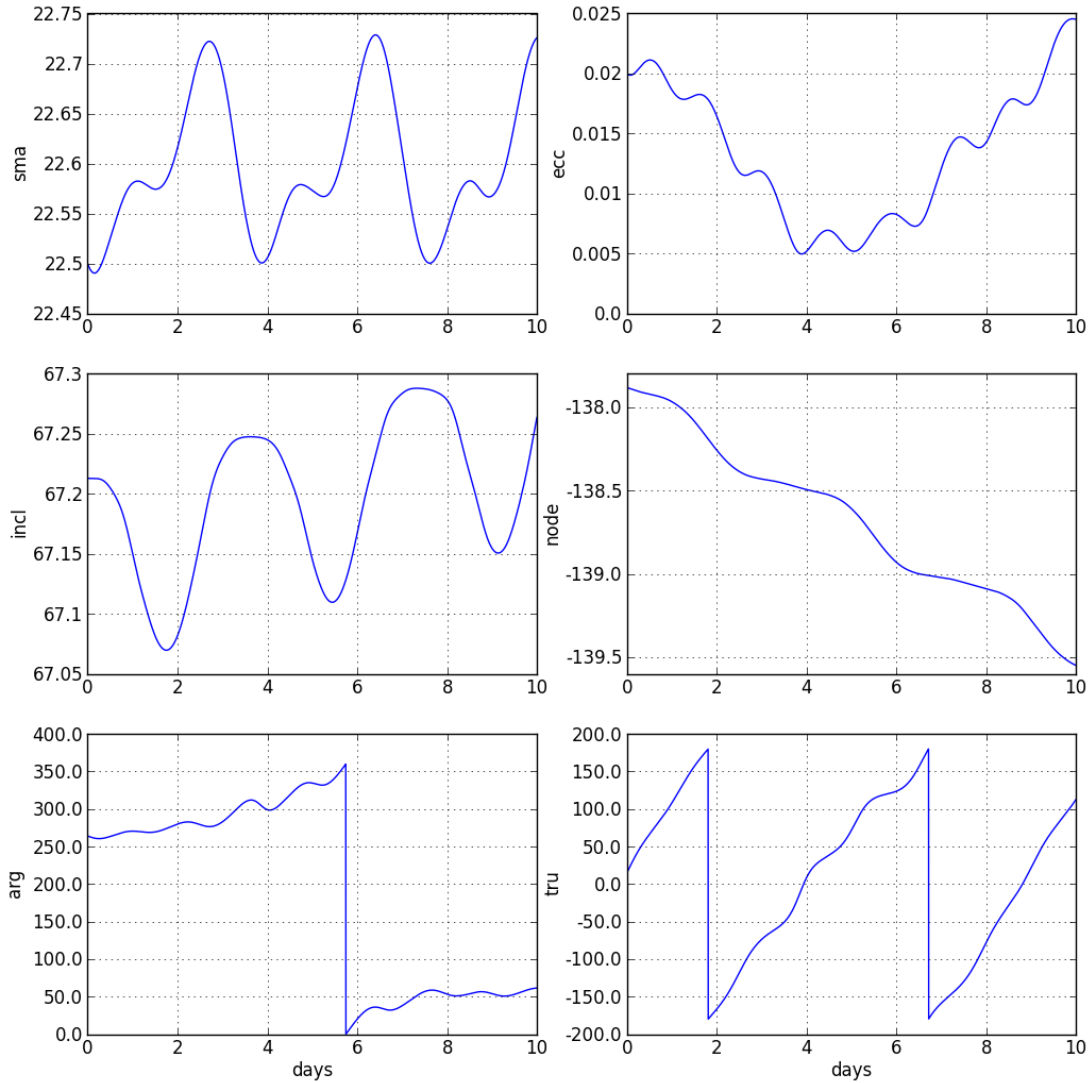


**Figure 1: Evolution of the Keplerian orbital elements (Sun Line Frame) over a 10-day propagation**

Over the 10-day test propagation, it was determined that  $C_g$  was indeed nearly constant, as shown in Figure 2. There is a less than 3% variation peak-to-trough, with a pronounced secular trend. Fortunately, this is easy to explain, as Tempel 1 is on the inbound half of its orbit over these 10 days, dropping from 4.02 AU to 3.99 AU, increasing the solar pressure acceleration from  $19.9 \text{ nm/s}^2$  to  $20.2 \text{ nm/s}^2$ , or a 1.5% increase. This is sufficiently flat that, as shown in Figure 3, the initial value alone is good enough to capture the long-period evolution of the orbit in  $e-\omega$  space.

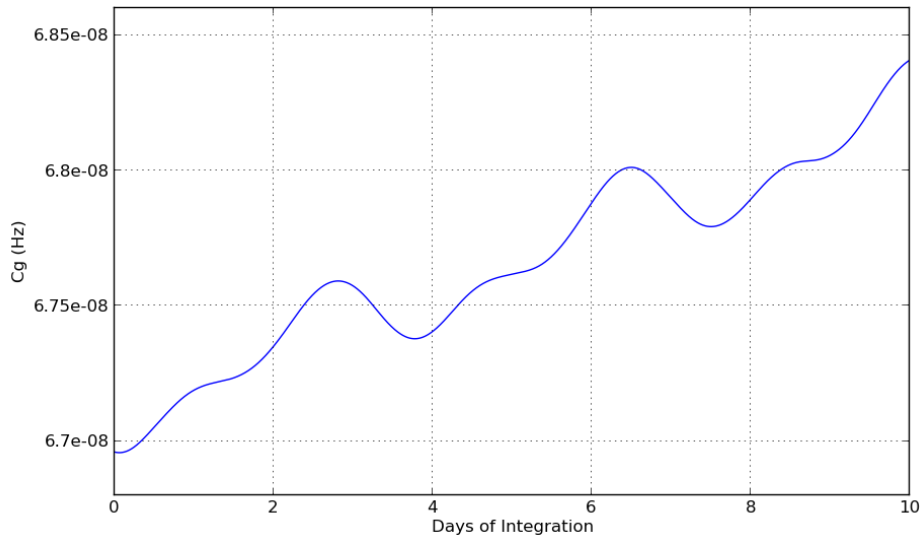


Figure 2: SRP/Gravity Parameter vs. Time

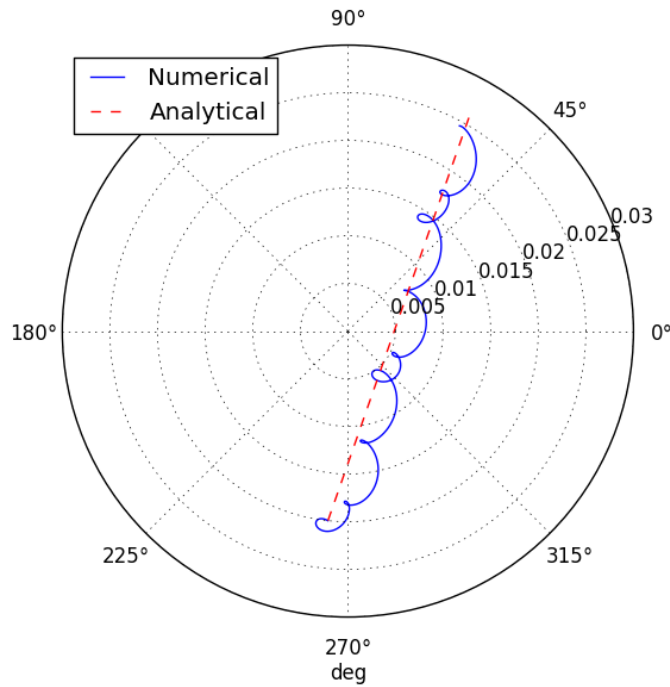


Figure 3: The motion of the fully integrated trajectory within  $e$ - $\omega$  space (blue, solid) compares nicely with the approximation of the derived control law (red, dashed).

### CHOOSING AN INITIAL ECCENTRICITY AND ARGUMENT OF PERIAPSIS

To maximize the time between maneuvers, the initial argument of periapsis ( $\omega_0$ ) should be a value that puts the modeled motion in  $e$ - $\omega$  space (the red dashed line in Figure 3) through the origin, as in Equation 25.

$$\omega_0 = \pi + \tan^{-1}\left(\frac{-C_g \cos \lambda}{-C_g \cos i \sin \lambda}\right) = \pi + \tan^{-1}\left(\frac{-\cos \lambda}{-\cos i \sin \lambda}\right) \quad (25)$$

When solving for the inverse tangent, the quadrant of the solution should be retained. As in Figure 3, the initial argument could easily be in Quadrant III ( $180^\circ \leq \omega_0 \leq 270^\circ$ ). Most numerical packages contain a version of the inverse tangent that retains the quadrant, typically called “atan2.” The negative signs are thus preserved in Equation 25, as “atan2” routines separate out the numerator and denominator of the inverse tangent and that information must be preserved.

Using the values from Table 1, Equation 25 states that the optimal initial argument of periapsis, in the sun-line frame for our Tempel 1 example, is 250.7 deg, very similar to Table 1’s 264.0 deg. As expected, by inspection of Figure 3, this optimal location is to the left of, or clockwise from, the initial point defined by the state in Table 1.

One rather interesting implication of Equation 25 is that the size and shape of the orbit, the mass of the asteroid, and the solar distance are all irrelevant to the selection of the argument of periapsis target. The maneuver frequency is a function of those parameters, but the optimal initial argument of periapsis is not. Since the inclination and argument of node are essentially fixed (per Equations 11 and 12), the evolution of the optimal initial argument of periapsis is a simple function of the position of the asteroid about the sun. For mission durations much smaller than the heliocentric orbit period, a single fixed value of  $\omega_0$  is an appropriate approach. For longer missions, the controller will eventually fail when the cosine of the hour angle changes sign and the motion within  $e$ - $\omega$  space reverses itself. This shortcoming is easily circumvented by manually updating the  $e$ - $\omega$  target as a function of mission timeline.

The selection of the initial eccentricity can be a function of the mission objective, such as keeping the variation in the orbital altitude below some limit, or designed to meet some particular maneuver frequency. If a particular maneuver frequency is desired, then Equations 22 and 23 can be recombined to give a total eccentricity rate, as in Equation 26:

$$\dot{e} = C_g \sqrt{1 - \sin^2 \lambda \sin^2 i}. \quad (26)$$

This equation is not the same as Equation 3. This rate is subject to all of the various near-circular assumptions made in the derivations of Equations 22 and 23. However, it is useful in that it models how fast the orbit evolves along the red dashed line in Figure 3 defined by Equations 22 and 23. As such, if some particular duration,  $t_m$ , is desired between maneuvers, the initial eccentricity should be as in Equation 27. Equivalently, the estimated time between maneuvers, given some initial eccentricity, is as in Equation 28. These two equations can help bound the trade between orbital eccentricity and operational tempo.

$$e_0 = \frac{t_m C_g}{2} \sqrt{1 - \sin^2 \lambda \sin^2 i} \quad (27)$$

$$t_m = \frac{2e_0}{C_g \sqrt{1 - \sin^2 \lambda \sin^2 i}} \quad (28)$$

Using the value of the initial eccentricity of 0.02 from Table 1, Equation 28 suggests that the spacecraft would exceed an eccentricity of 0.02 after 8.8 days, which is what the upper-right panel of Figure 1 shows.

## THE FIXED-TARGET CONTROLLER

The first controller designed using the above dynamics was a simple, single-impulse controller that returns the eccentricity ( $e$ ) and argument of periapsis ( $\omega$ ) to some fixed user-specified and Equations 25-28 informed value. The controller achieves this by searching for when a constraint is violated and then applying the corrective maneuver at the last opportunity to do so before the violation was encountered. This fixed-target and maneuver-before-violation approach results in a

variable duration between maneuvers. The intent is that this controller would be used when the maximum eccentricity matters more to the mission objective and concept-of-operations than the operations tempo.

The fixed-target controller propagates an initial state forward in time until either a constraint is violated or a fixed time has elapsed. If the fixed time is encountered, then the simulation is said to be complete and no further integrations are undertaken. If a constraint violation is found, the controller searches for when, prior to the violation, a single maneuver could have been performed to return the orbit evolution to the user-specified eccentricity,  $e_s$ , and argument of periapsis,  $\omega_s$ . This is accomplished by searching for when Equation 29 is satisfied.

$$r = \frac{a(1-e_s^2)}{1-e_s \cos(\omega+f-\omega_s)} \quad (29)$$

where  $a$ ,  $r$ ,  $\omega$ , and  $f$  are the instantaneous semi-major axis, orbital radius, argument of periapsis, and true anomaly of the pre-maneuver state, respectively. The maneuver vector is then simply determined by solving for the Cartesian states of the desired orbit using the pre-maneuver instantaneous inclination and longitude of node and then differencing the velocity component from the pre-maneuver Cartesian velocity. This formulation preserves the orbit size and plane while re-shaping and re-orienting the orbit to match the desired values.

Using the initial conditions from Table 1, the fixed target controller was run for 365 days using an  $e = 0.02$ ,  $\omega = 250.7$  deg target and a two-sided range constraint. The range between the spacecraft and the comet center was required to remain between 22 and 23 km. The results are illustrated in Figures 4-8. As can be seen in Figure 6, the controller does an excellent job of maintaining the orbital radius within its designated bounds. The variation, particularly in the second half of the integration is apparently too tight, suggesting that that controller might be doing maneuvers earlier than necessary. However, that is a feature of a single-maneuver controller. At the next opportunity in the orbit where Equation 29 holds, the orbital radius would have exceeded its bounds, and so the achieved variability is less than the requirement. The total delta-v for this was small: about 1.4 m/s total.

These figures illustrate the fundamental short-coming of this controller as implemented, though. As the hour angle (“node”) of the orbit changes, the ratio  $\dot{e}_y/\dot{e}_x$  changes and the  $e$ - $\omega$  evolution slowly rotates counter-clockwise. Because the maneuvers are triggered by the orbital radius exceeding or dropping below fixed values, the time between maneuvers gets shorter and shorter. By the end of the 365-day integration, the maneuver spacing has dropped from slightly over 7 days to just over 3.5 days. As the node continues to change due to Tempel-1’s motion about the sun, the maneuver frequency will continue to increase. Eventually, the sign  $\dot{e}_y$  will change and the constraints will be violated almost immediately.

One additional feature of note is the time history of the inclination. The near-circular assumption of  $e \approx 0$ , transforming Equation 2 into Equation 11, states that the inclination should be constant. That is clearly not the case, as the inclination has increased from 67 deg to 71.25 deg over the course of a year. However, the rate of change in the inclination is an order of magnitude slower than the rate of change in the argument of periapsis and thus Equation 11 remains a useful approximation, particularly as its implications are applied to the control law encoded in Equations 22-23 and 26-28.

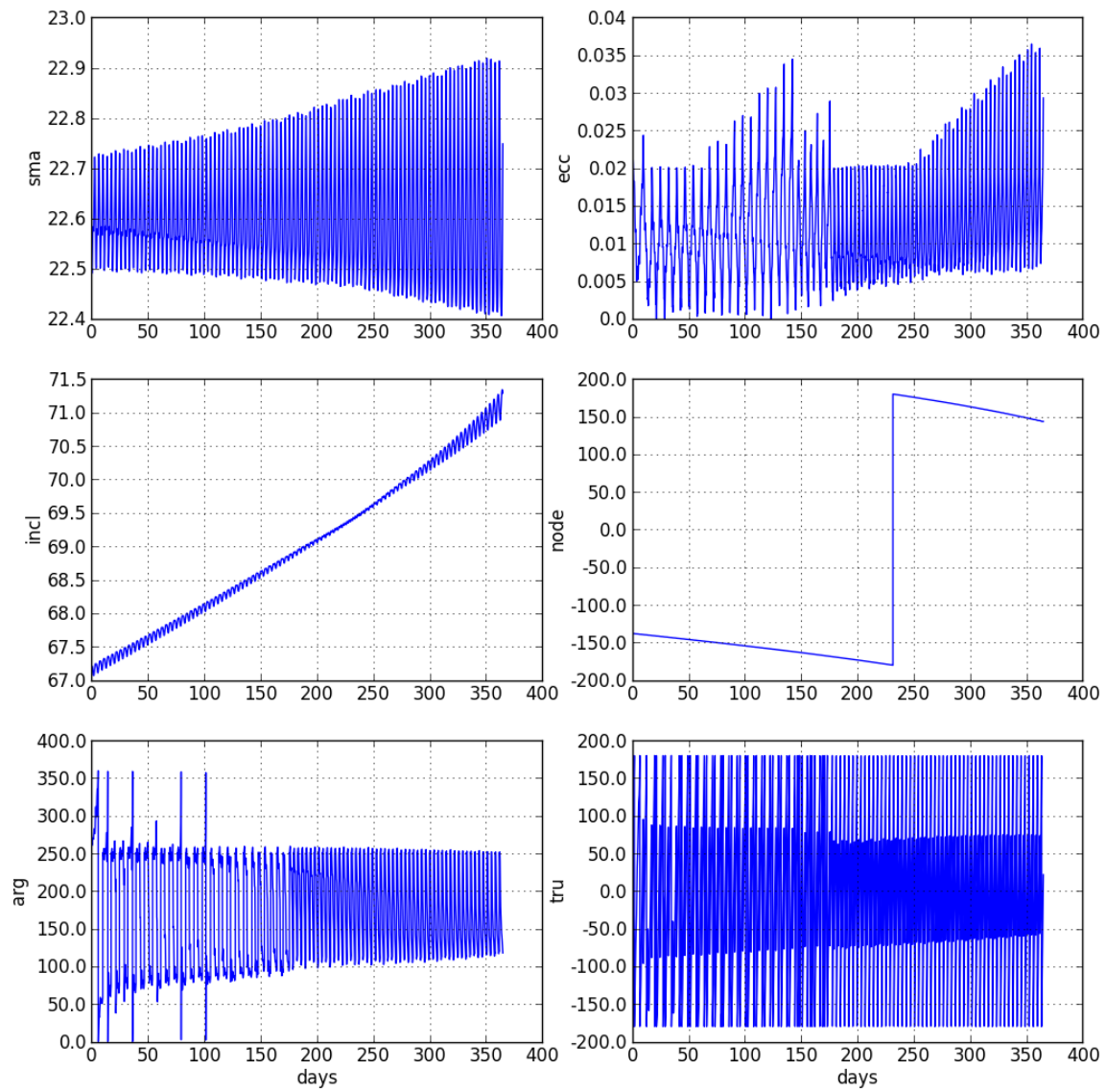


**Figure 4: Orbital Elements from a 365-day integration of the fixed-target controller.  
Note the growth in inclination (middle-left).**

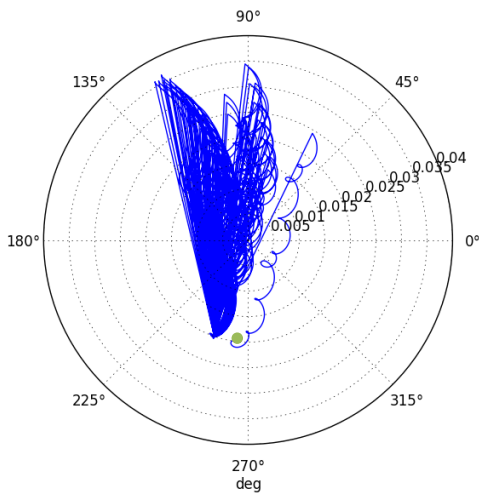


**Figure 5:** Polar plot of the eccentricity vector from a 365-day integration of the fixed-target controller (starting at the green dot). Note the counter-clockwise rotation of the trend as the node changes.

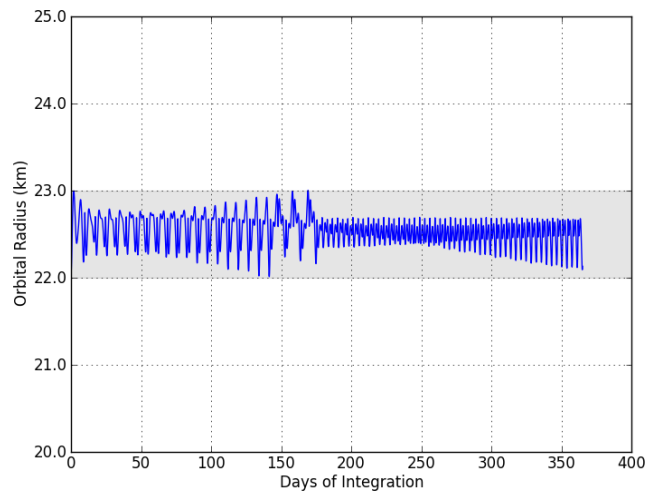


**Figure 6:** Time history of the orbital radius during a 365-day integration of the fixed-target controller. The controller maintains the 22-23 km constraint at the expense of variability in the ops tempo.

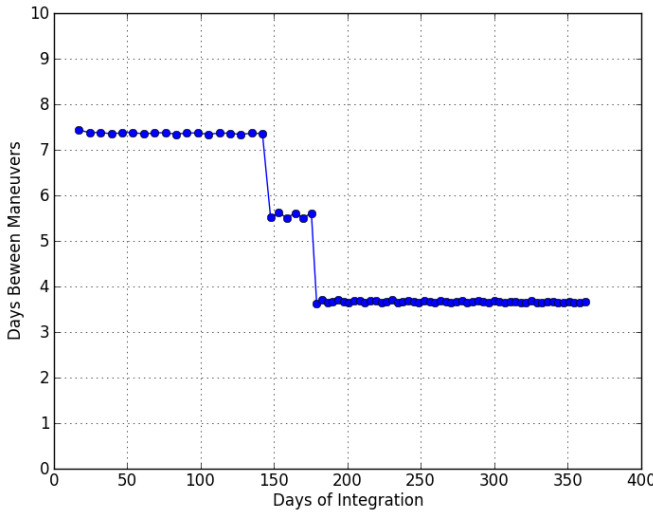


**Figure 7:** Days between Maneuvers during a 365-day integration of the fixed-target controller. As the  $e-w$  evolution rotates clockwise, the time between maneuvers gets shorter.

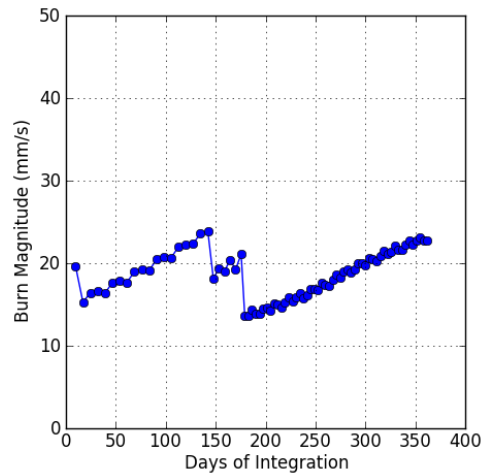


**Figure 8:** Maneuver sizes during a 365-day integration of the fixed-target controller.

### THE FIXED-SCHEDULE CONTROLLER

The second controller designed was somewhat more complex. While it too is single impulse, the controller chooses its own eccentricity and argument of periapsis targets to keep the orbit as circular as possible with a constant time between maneuvers. “Constant” in this case is a relative term. Because single-impulse maneuver opportunities only occur when Equation 29 is satisfied, there is necessarily some variability involved in the maneuver timing. There are many ways to accommodate that fact. This controller propagates for a fixed duration and finds the opportunity to do a maneuver prior to the end of that duration in much the same way as the fixed-target

controller. It is essentially a temporal constraint instead of a spatial constraint. The eccentricity and argument of periapsis targets for Equation 29 are determined using Equations 27 and 25 based on the instantaneous values for the inclination,  $i$ , hour angle,  $\lambda$ , and SRP/gravity parameter,  $C_g$ , at the end of the propagation and a user-specified desired maneuver interval,  $t_m$ . The pre-integration duration and desired maneuver interval are somewhat independent.

Using the initial conditions from Table 1, the fixed-schedule controller was run for 365 days using an initial propagation time of 8 days and a desired maneuver interval of 7 days. The results are illustrated in Figures 9-13. As can be seen in Figure 11, the controller does a very good job of maintaining a nearly constant maneuver frequency: 7.4-7.5 days between maneuvers. Careful tuning of the orbit size and inputs to the control law should allow an operations-friendly maneuver frequency to be selected.

The increasing eccentricities in Figure 9 and orbital distances in Figure 11 illustrate how this controller maintains a nearly-constant maneuver schedule. As Tempel 1 closes with the Sun and the SRP/gravity parameter,  $C_g$ , rises, the eccentricity rate increases and the orbit's initial eccentricity must increase with it. This is can be seen very clearly in Figure 10 as the initial and final eccentricities move radially outwards. This also has an effect on the per-maneuver sizes. As the maneuvers are forced to move the orbiter ever-further in  $e-\omega$  space, they get ever larger. The total is almost identical to the fixed-target controller because the maneuver frequency is (more) constant, however: about 1.4 m/s.

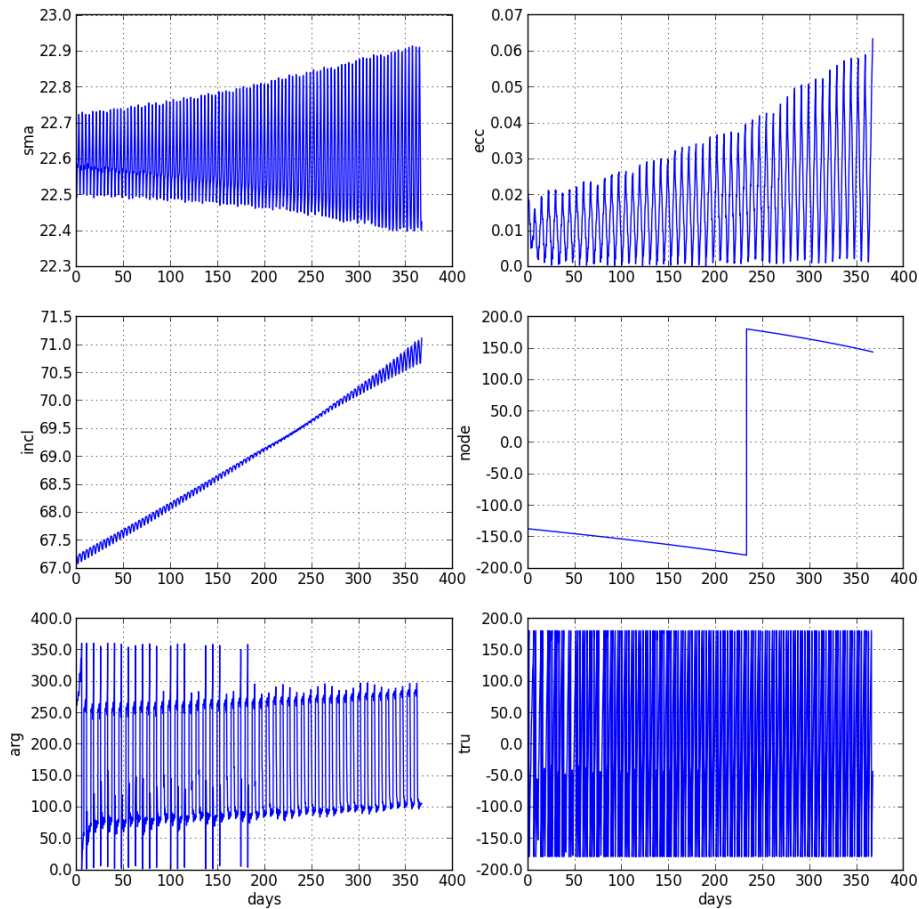


**Figure 9: Orbital Elements from a 365-day integration of the fixed-schedule controller.**

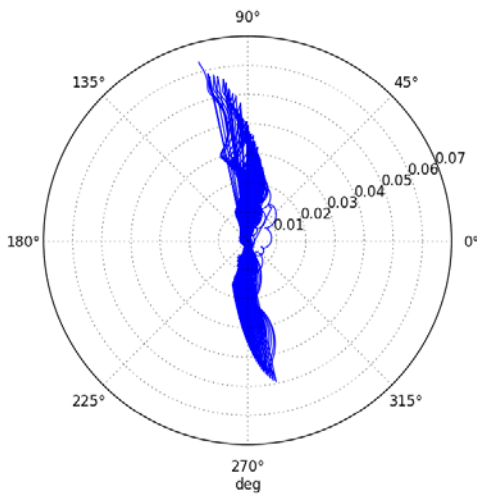


**Figure 10: Polar plot of the eccentricity vector from a 365-day integration of the fixed-schedule controller. Note the counter-clockwise rotation of the initial argument of periapsis as the ascending node changes (middle-right panel of Figure 9).**

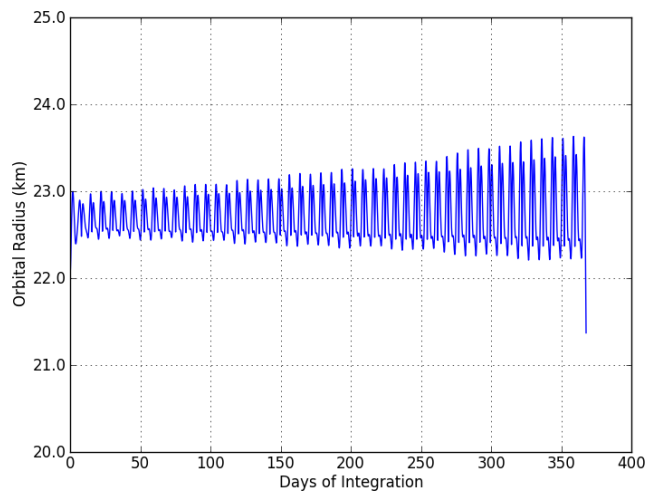


**Figure 11: Time history of the orbital radius during a 365-day integration of the fixed-schedule controller. The near-constant ops tempo comes at the expense of growing orbital radius variation.**

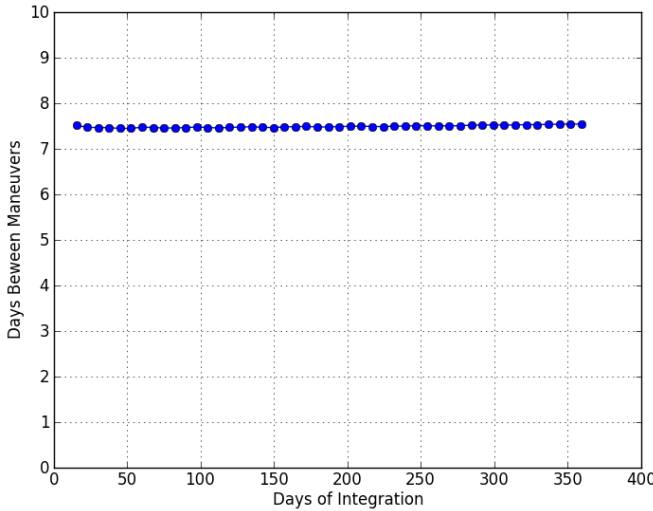


**Figure 12: Days between Maneuvers for a 365-day integration of the fixed-schedule controller. The variability is 7.4-7.5 days between maneuvers.**

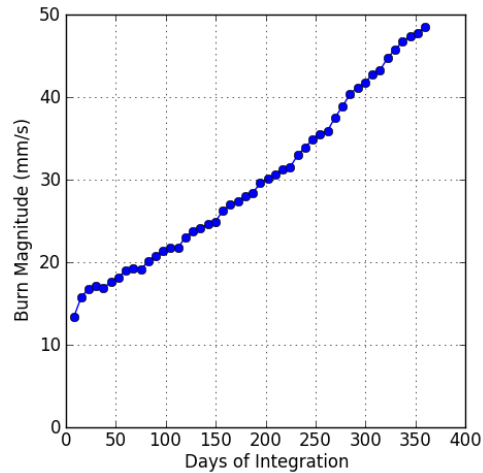


**Figure 13: Maneuver sizes during a 365-day integration of the fixed-schedule controller.**

## CONCLUSIONS AND FUTURE WORK

The two control-laws using the analytical results of Equations 22-23, 24-25, and 27-28 are numerically simple but very powerful. The fixed schedule controller, in particular, is extraordinarily stable. During testing, it was able to maintain an orbit about Tempel 1 through perihelion and the relatively high solar-radiation-pressure environment. With proper tuning, this controller may be able to meet most orbital maintenance requirements for a near-circular orbit about a primitive body.

Other implementations, such as a controller that maintains a fixed orbital distance like the example fixed-target controller, but with the adaptability and stability of the fixed-schedule controller could also be built. Another option might be to use the orbital radius constraint and fixed-initial-eccentricity of the fixed-target controller with the variable initial argument of the fixed-schedule controller to capture the rotation of the  $e-\omega$  space evolution. The fixed-target controller's stability could also be improved by combining it with an out-of-plane controller to maintain the hour angle at a near-constant value.

## ACKNOWLEDGMENTS

This research was carried out at the Jet Propulsion Laboratory, California Institute of Technology, under contract with NASA.

## REFERENCES

<sup>1</sup> Scheeres, D.J. "Satellite Dynamics About Asteroids" AAS 94-112

<sup>2</sup> <http://ssd.jpl.nasa.gov/?horizons>, retrieved 28 August 2012

<sup>3</sup> Thomas, Peter C., et al., "The shape, topography, and geology of Tempel 1 from Deep Impact observations" *Icarus*, Vol. 191, 2007, pp. 51-62.

<sup>4</sup> Werner, R.A. "The Gravitational Potential of a Homogenous Polyhedron, or Don't Cut Corners," *Celestial Mechanics & Dynamical Astronomy*, Vol. 59, 1994, pp. 253-278.